Infrared Studies of Carbon Monoxide Binding to Carbon Monoxide Dehydrogenase/Acetyl-CoA Synthase from *Moorella thermoacetica*†

Jingyi Chen,‡ Shan Huang,‡ Javier Seravalli,§ Howard Gutzman, Jr.,‡ Derrick J. Swartz,‡ Stephen W. Ragsdale,§ and Kimberly A. Bagley*,‡

Department of Chemistry, Buffalo State, State University of New York, Buffalo, New York 14222, and Department of Biochemistry, Beadle Center, University of Nebraska, Lincoln, Nebraska 68588

Received June 3, 2003; Revised Manuscript Received October 3, 2003

ABSTRACT: Carbon monoxide dehydrogenase/acetyl-CoA synthase (CODH/ACS) is a bifunctional enzyme that catalyzes the reversible reduction of carbon dioxide into carbon monoxide and the coupled synthesis of acetyl-CoA from the carbon monoxide produced. Exposure of CODH/ACS from *Moorella thermoacetica* to carbon monoxide gives rise to several infrared bands in the 2100−1900 cm^{-1} spectral region that are attributed to the formation of metal-coordinated carbon monoxide species. Infrared bands attributable to M−CO are not detected in the as-isolated enzyme, suggesting that the enzyme does not contain intrinsic metal-coordinated CO ligands. A band detected at 1996 cm^{-1} in the CO-flushed enzyme is assigned as arising from CO binding to a metal center in cluster A of the ACS subunit. The frequency of this band is most consistent with it arising from a terminally coordinated Ni(I) carbonyl. Multiple infrared bands at 2078, 2044, 1970, 1959, and 1901 cm^{-1} are attributed to CO binding at cluster C of the CODH subunit. All infrared bands attributed to metal carbonyls decay in a time-dependent fashion as CO_2 appears in the solution. These observations are consistent with the enzyme-catalyzed oxidation of carbon monoxide until it is completely depleted from solution during the course of the experiments.

The bifunctional enzyme carbon monoxide dehydrogenase/acetyl-CoA synthase (CODH/ACS),[1] the key component of the Wood−Ljungdahl pathway of anaerobic CO_2 fixation, is a macromolecular machine that consists of two subunits (*1*, *2*). This 300 kDa $\alpha_2\beta_2$ protein, which contains two core CODH β subunits tethered on each side to two ACS α subunits, is studded with metals (2−3 Ni, 14 Fe, as well as Cu and Zn) that are arranged into four metal clusters (*3*, *4*). The CODH subunit catalyzes the two-electron reduction of CO_2 to CO at a novel $NiFe_4S_{4-5}$ cluster called cluster C. The two electrons, which are ultimately derived, through ferredoxin, from one of several cellular reductants, including H_2/hydrogenase or pyruvate/pyruvate:ferredoxin oxidoreductase, are transferred to cluster C from cluster B, a typical [4Fe-4S] cluster, which apparently receives its electrons from cluster D (a [4Fe-4S] cluster that bridges the two β subunits). These electron-transfer reactions are reversed in the monofunctional CODH, which catalyzes oxidation of CO to CO_2, thereby removing this toxic gas from the atmosphere and providing low-potential electrons for reduction of cellular components. CO oxidation is also linked to generation of ATP through electron transport linked generation of a protonmotive force (*5*). CO removal is important because it is a toxic gas that is released to the global atmosphere by natural and anthropogenic sources at a rate of about 2600 Tg (3×10^9 tons) per year (*6*, *7*), leading to atmospheric CO concentrations ranging from ∼0.1 ppm in rural to 200 ppm in urban settings (*8*). CO is toxic to animals because it binds to essential metalloproteins, such as cytochrome oxidase. Soil microbes exploit CO as a carbon and energy source (*1*, *9*) and, using CODH, can remove this toxic gas from the environment at a rate of about 300 Tg (3×10^8 tons) per year (*6*, *7*).

In anaerobic microbes that use the Wood−Ljungdahl pathway, the CODH subunit is tightly bound to the ACS subunit and permits the CO, generated at the C cluster of CODH, to be utilized as a metabolic intermediate during growth on CO_2 or organic carbon sources (*10*). Another unique feature of this pathway is that intermediates are tightly bound to enzymes in a bioorganometallic reaction sequence (*1*, *2*, *11*). In the Wood−Ljungdahl pathway, after CODH reduces CO_2 to CO, the CO travels through a 70 Å channel from cluster C to cluster A in ACS, where it combines with a methyl group and CoA to generate acetyl-CoA (*3*, *4*). Cluster A, the active site of ACS, is a [4Fe-4S] cluster that is bridged by a cysteinyl sulfur (Cys^{509}) to the proximal metal of a binuclear center, which contains a proximal metal (Cu, Ni, or Zn) and a square-planar nickel ion (the *distal Ni*) in an N_2S_2 ligand environment consisting of the side chains of Cys^{595} and Cys^{597} and the backbone N atoms of Gly^{596} and Cys^{597} (*3*, *4*). Thus, in one structure, the [4Fe-4S] cluster is bridged to a CuNi binuclear center (*4*), while, in the other, it is bridged to either a NiNi or a ZnNi site (*3*).

† This research is supported by NSF Grant MCB-0130905 (K.A.B.) and NIH Grant GM39451 (S.W.R.).

* To whom correspondence should be addressed. E-mail: bagleyka@buffalostate.edu. Phone: (716) 878-5933. Fax: (716) 878-4028.

‡ Buffalo State.

§ University of Nebraska.

[1] Abbreviations: CODH, carbon monoxide dehydrogenase; ACS, acetyl-CoA synthase; IR, infrared; FTIR, Fourier transform infrared; Mb, myoglobin; EDTA, ethylenediaminetetraacetic acid; Tris, 2-amino-2-(hydroxymethyl)-1,3-propanediol; DTT, dithiothreitol; ophen, *o*-phenanthroline; EPR, electron paramagnetic resonance.

10.1021/bi0349470 CCC: $25.00
Published on Web 11/25/2003

Infrared (IR) spectroscopy is an obvious and incisive method to study CO binding to CODH/ACS since there are catalytically important CO binding sites on the various reduced metal centers of both the C and A clusters. A single IR absorption peak at 1996 cm^{-1} has been assigned to the ν(CO) for CO binding at cluster A of ACS on the basis of several criteria (see the Discussion section) (*12*), yet until now, there have been no further reported IR studies of CODH or ACS. Interestingly, multiple IR bands arising from CO seem to be the rule, rather than the exception, in metalloproteins containing CO as a ligand, even when there is a single CO binding site. The system that is most similar to CODH is the NiFe hydrogenase, which contains a single CO but exhibits multiple M−CO vibrations, depending on redox state (from 1900 to 1980 cm^{-1}) (*13*−*15*). A related system is the Fe-only hydrogenase, containing three intrinsic CO's bound to a diiron subsite, two of which are terminally coordinated and one bridges the two Fe's of the 2Fe subcluster. This results in three ν(CO) bands ranging from 1801 to 2017 cm^{-1}, with frequencies that are dependent on the conformation and redox states of the active site (*16*−*18*). IR spectroscopy has also been used to study other proteins that bind CO, including heme proteins such as myoglobin (Mb), hemoglobin, and cytochrome oxidase. The IR spectrum of the CO stretching mode of Mb−CO has three major absorption bands, with peaks at 1965, 1944, and 1932 cm^{-1} (*19*−*21*), which are assigned to Fe(II)−CO vibrations experiencing different conformations of the heme pocket residues (*22*). Cytochrome oxidase exhibits discrete peaks for the transient Cu_B(I)−CO intermediate (2063 cm^{-1}) and for the Fe(II)−CO (from heme a_3, two conformers with peaks at 1964 and 1945 cm^{-1}) species (*23*).

Here we describe IR results for the metal−carbonyl complexes on CODH/ACS from *Moorella thermoacetica* that form upon exposure of the enzyme to carbon monoxide. A single band at 1996 cm^{-1} is assigned to a terminal carbonyl bound to cluster A of ACS. Multiple bands at 2074, 2044, 1970, 1959, and 1901 cm^{-1} are assigned to terminal carbonyls bound to a metal center(s) at cluster C of CODH. These metal−carbonyl bands disappear as CO undergoes oxidation to CO_2, which depletes bound CO from the enzyme.

MATERIALS AND METHODS

CODH/ACS was isolated and purified from *M. thermoacetica* (formerly *Clostridium thermoaceticum*) as previously described (*24*, *25*). Protein purification and sample preparations prior to IR spectroscopy were carried out inside an anaerobic chamber (Vacuum Atmospheres, Hawthorne, CA) containing <1 ppm of O_2 as measured continuously with an oxygen analyzer (Teledyne, City of Industry, CA).

The enzyme, equilibrated in 100 mM Tris-HCl, pH 7.60, with 2 mM dithiothreitol (DTT), was concentrated to a final concentration of ~0.66 mM by using a stirred cell concentrator with a YM30 membrane (Amicon) followed by YM30 nanoconcentrator filters (Filtron), loaded into an anaerobic vial under nitrogen and then frozen and stored at −80 °C prior to performing the experiments described herein. Treatment of CODH/ACS with *o*-phenanthroline (ophen), essentially as described earlier (*26*, *27*), was accomplished by addition of 10 equiv of ophen per $\alpha\beta$ CODH/ACS heterodimer to the enzyme until the NiFeC EPR signal associated with CO binding to cluster A was significantly reduced. Excess ophen was removed by three cycles of concentration/dilution (>10-fold each cycle) with 0.1 M Tris-HCl, pH 7.60, and 2 mM DTT (final concentration of ophen was below 1 μM). After the ophen treatment, the enzyme exhibited approximately 16% of the original NiFeC signal and approximately 5% of the specific activity in the CO/[1-^{14}C]-acetyl-CoA exchange reaction (*28*) compared to the untreated CODH/ACS. In contrast, the CO oxidation activity (*25*) was not significantly altered by this procedure (380 μmol min^{-1} mg^{-1} for ophen-treated enzyme and 436 μmol min^{-1} mg^{-1} for untreated enzyme). Treatment with EDTA was accomplished by exchanging the enzyme into 10 mM EDTA, 100 mM Tris-HCl, pH 7.6, and 2 mM DTT by concentration and dilution with an Amicon ultrafiltration unit.

For EPR experiments, CO was passed above a solution of 0.1 mM CODH/ACS in 100 mM MES and 2 mM DTT in D_2O (pD 6.5) in a N_2-filled anaerobic vial. After 15 min of flushing with CO, a 200 μL aliquot was transferred into a sealed quartz X-band EPR tube inside the anaerobic chamber (<1 ppm O_2) using a gastight Hamilton syringe with a 12 in. long needle. The EPR sample was frozen within 1 min by dousing the tube in a solution of liquid isopentane maintained at 143 K by adding liquid nitrogen. For each subsequent time point, the sample was thawed, incubated at room temperature (293 K), and refrozen as just described, and the EPR spectrum was recorded at 77 K with the following instrument parameters: power, 4.0 mW; gain, 20000; modulation amplitude, 10.145 G; modulation frequency, 100 kHz. The height of the S-shaped 2.07 feature of the NiFeC signal was plotted versus time in Figure 3. The sample that was frozen 1 min after incubation with CO contained 0.28 NiFeC spin per mole of $\alpha\beta$ heterodimer.

For the infrared experiments using natural abundance CO, the enzyme was thawed in the anaerobic vial in which it had been stored, placed in an ice water bath, and then flushed for 5 min with CO. CO (natural abundance, grade 4.0 from Air Products Inc.) was passed through an OxyClear cartridge (DGP-250-1) to remove residual oxygen and then introduced into the sample using a needle through the vial's septum while simultaneously venting with a second needle. After flushing for 5 min with CO, the venting needle was removed, and a slight overpressure of CO (1−3 psi) was added to the vial before the second needle was removed. For the ^{13}CO-flushed enzyme, the vial was immersed in an ice water bath, and the enzyme was alternately degassed under vacuum and flushed with ^{13}CO for a total of 8−10 cycles, ending with a slight overpressure of ^{13}CO gas. The ^{13}CO gas contained greater than 99% ^{13}CO with less that 1% ^{18}O (Cambridge Isotopes). The CO- (^{13}CO-) flushed enzyme was then immediately loaded into an anaerobic cell that had been flushed with CO (^{13}CO). Loading the sample into the anaerobic IR cell was done using a gastight Hamilton syringe while inside a COY anaerobic chamber containing 1−3% H_2 (residual nitrogen and <1 ppm of O_2). The anaerobic IR cells used in these experiments were equipped with IR transmitting windows made of CaF_2 and had an approximate optical path length of 50 μm. The total sample volume in these cells was approximately 15 μL. Infrared spectra were collected at room temperature using a Bio-Rad FTS-40A

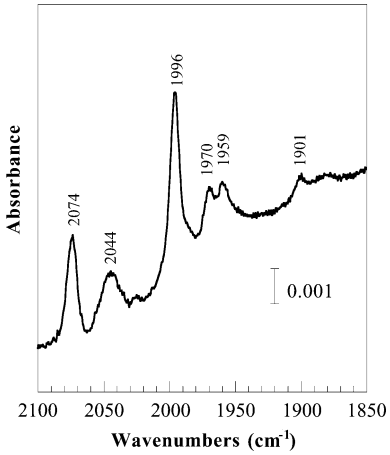

FIGURE 1: Infrared spectrum of CODH/ACS from *M. thermoacetica* after being flushed with natural abundance CO. The enzyme concentration was 0.57 mM in 100 mM Tris-HCl buffer, pH 7.60, with 2 mM DTT. The spectrum was taken 5 min after the IR cell was loaded. The spectrum represents an average of 10 scans. The baselines were not corrected, nor were the spectra smoothed. However, IR bands arising from the vibration−rotation of water vapor were subtracted using a reference spectra of water vapor.

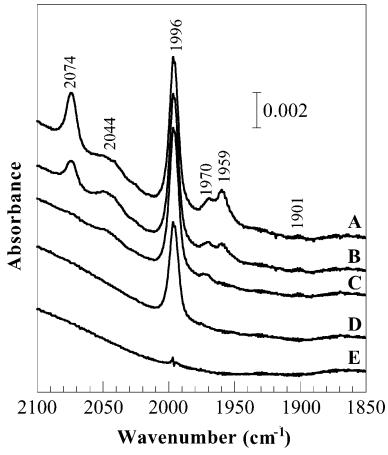

FIGURE 2: IR spectra of CO-flushed CODH/ACS taken (A) 5 min, (B) 60 min, (C) 115 min, (D) 170 min, and (E) 6 h after the IR cell was loaded. The sample was flushed with CO and then immediately loaded into the IR cell. Spectra represent the average of 512 scans at 1 cm^{-1} resolution and were taken at room temperature. The baselines were not corrected, nor were the spectra smoothed. However, IR bands arising from the vibration−rotation of water vapor were subtracted from spectra taken at early times (<2 h). The enzyme concentration was 0.60 mM.

FTIR spectrometer equipped with an HgCdTe (MCT) detector with a spectral resolution of 1 cm^{-1}.

Simulations of IR and EPR Decay Data. The program KINSIM/FITSIM (*29*) was used to simulate and fit the data corresponding to the 2044 and 1996 cm^{-1} IR bands and the S-shaped $g = 2.07$ component of the EPR spectrum. The kinetic model for the observed lag and subsequent decay of the 1996 cm^{-1} and $g = 2.07$ intensities assumes that free CO is initially present in solution at 1.0 mM concentration at room temperature (CO solubility) and is depleted by oxidation of CO to CO_2 and H_2. After the CO-treated CODH/ACS was loaded into either the IR cell or the nitrogen-filled EPR tube, a steady-state cycle is established in which CODH is reduced by CO (with formation of CO_2 in step 1) followed by electron transfer to protons in solution (with formation of hydrogen in step 2). The ACS−CO complex (eq 3), which corresponds to the 1996 cm^{-1} IR band and the $g = 2.07$ EPR signal, decays as CO is depleted from the solution. The initial intensities were calculated by dividing the maximal observed intensities in either IR or EPR by the concentration of ACS. The decay of the 1996 cm^{-1} band was used to fit the forward and reverse rate constants for eqs 1−3. The decay of the NiFeC signal was fitted using the rate constants for eqs 1−3 obtained from the 1996 cm^{-1} fit. The same fitting procedure was employed for the 2044 cm^{-1} band but allowing variation in the rate constants for eq 3. The output traces are plotted in Figure 3.

$$CODH_{ox} + CO + H_2O \rightleftarrows CODH_{red} + CO_2 + 2H^+ \quad (1)$$

$$CODH_{red} + 2H^+ \rightleftarrows CODH_{ox} + H_2 \quad (2)$$

$$ACS{-}CO \rightleftarrows ACS + CO \quad (3)$$

RESULTS

Infrared Spectra for the 2100−1800 cm^{-1} Region. Incubation of *M. thermoacetica* CODH/ACS with (natural abundance) CO gives rise to an infrared absorbance spectrum (Figure 1) with strong bands at 2074, 2044, 1996, 1970, 1959, and 1901 cm^{-1}. In contrast, enzyme that has not been exposed to CO prior to the cell being loaded does not exhibit any detectable IR bands in the 2100−1800 cm^{-1} spectral region, nor were any of these bands detected if the buffer alone was flushed with CO or if the IR cell itself was filled with CO gas. The latter observations rule out the possibility that these bands arise from nonspecific binding of CO to the IR cell. Initially, we were puzzled by what appeared to be a preparation-to-preparation variation in the relative intensity of these IR bands; i.e., the 2074 and 1996 cm^{-1} bands were detected with significant intensity in most preparations, but the bands at 2044, 1970, 1959, and 1901 cm^{-1} varied significantly in intensity from one preparation to the other. However, it was then found that the intensity of the bands depended on how much time had elapsed between flushing the enzyme with CO and collecting data in the IR cell. There is a time-dependent decay of all the infrared bands in the 2100−1800 cm^{-1} spectral region (Figure 2). Figure 3 shows the intensity of the IR bands detected in the CO-flushed enzyme as a function of time after the IR cell is loaded for a typical experiment. In all preparations studied, first the 2074 cm^{-1} band disappeared followed by the gradual disappearance of the other IR bands. The 1996 cm^{-1} band begins to decay only after all the other bands have disappeared. Incubating the enzyme under CO for varying lengths of time (1−2 h) in an anaerobic vial (filled with a CO headspace with a volume that is over 100 times greater than the sample volume) prior to loading the IR cell does not affect the rate at which the IR bands disappear; it is the elapsed time after the IR cell is loaded (which lacks a headspace) that is critical. Incubating the enzyme in a solution of 10 mM EDTA and 100 mM Tris-HCl (pH 7.6) or exchanging the enzyme into a pH 6.0 buffer (100 mM MES, pH 6.0) prior to flushing the enzyme with CO also does not significantly change the pattern of infrared bands detected (spectra not shown) or their rate of decay.

Incubating CODH/ACS in CO gives rise to a slowly relaxing EPR signal with g values of 2.08, 2.07, and 2.03,

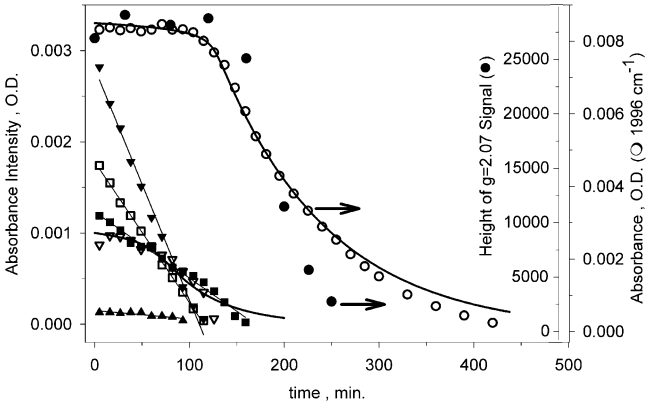

FIGURE 3: Time-dependent decay in intensity of the M−CO IR bands and the NiFeC EPR signal. Plots correspond to the intensities of the NiFeC signal (*g* 2.07, closed circles), 1996 cm^{-1} (open circles), 2074 cm^{-1} (closed triangles down), 2044 cm^{-1} (open triangles down), 1970 cm^{-1} (closed squares), 1959 cm^{-1} (open squares), and 1901 cm^{-1} (closed triangles up). The solid lines depict the fits of the 1996 and 2044 cm^{-1} band intensities and the NiFeC EPR signal intensity to the mechanism described by eqs 1−3 (see Materials and Methods) with the rate constants shown in the text or the fits to a linear decay curve for the other IR bands. The intensity of the IR bands detected in the 2100−1900 cm^{-1} spectral region was plotted as a function of time after CODH/ACS from *M. thermoacetica* was flushed with CO and then immediately loaded into the IR cell. IR spectra were taken at room temperature. The enzyme concentration was 0.60 mM. The time dependence of the NiFeC signal was measured under conditions in which CO is limited to what is in solution (see Material and Methods). *M. thermoacetica* CODH/ACS (100 mM in pH = 7.60, 2 mM DTT) showed 0.28 NiFeC spin per $\alpha\beta$ heterodimer. The X-band spectrum was recorded at liquid nitrogen temperature (77 K) with the following parameters: power, 4.0 mW; gain, 20000; modulation amplitude, 10.145 G; modulation frequency, 100 kHz. The EPR data were obtained from the amplitude of the S-shaped feature at $g = 2.07$.

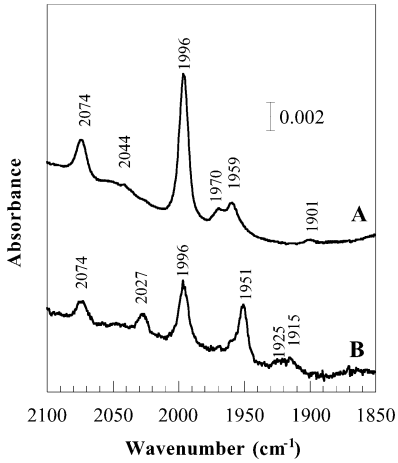

FIGURE 4: Infrared spectra of CODH/ACS from *M. thermoacetica* upon flushing with (A) natural abundance CO (primarily ^{12}CO) and (B) ^{13}CO (>99% ^{13}CO, <1% ^{18}O). Spectra were collected 5 min after the IR cell was loaded and represent an average of 512 scans at 1 cm^{-1} resolution. The baselines were not corrected, nor were the spectra smoothed. However, IR bands arising from the vibration−rotation of water vapor were subtracted from spectra. The enzyme concentration was 0.612 mM in 100 mM Tris-HCl buffer, pH 7.6, in 2 mM DDT.

termed the NiFeC signal, which is attributable to CO binding at cluster A (*30*). As seen in Figure 3, this CO-induced EPR signal decays under experimental conditions comparable to those used in the IR studies (without a CO gas phase; see Materials and Methods). When CODH/ACS is first flushed with CO and then transferred to an EPR tube under N_2, the NiFeC signal remains stable for approximately 120 min but then decays with a half-life of approximately 55 min (Figure 3), as was observed for the 1996 cm^{-1} IR band. The simulation of the decay curves for the NiFeC signal and the1996 cm^{-1} band yielded rate constants for the dissociation of CO (the decay step, eq 3) of $k_3 = \sim 0.27$ and ~ 0.29 min^{-1}, respectively, indicating that the 1996 cm^{-1} band is the IR signature of the paramagnetic complex between CO and the A cluster in the ACS subunit. Further experiments using ophen also support this assignment (vide infra). The fitted rate constant for CO-dependent reduction of CODH (k_1) is 30 mM^{-1} min^{-1}, while the rate constant for oxidation of the enzyme, concomitant with H_2 formation, k_2, is 0.018 mM^{-1} min^{-1}. The 2044 cm^{-1} band also shows a significant time lag, but its decay rate is faster (~ 1 min^{-1}).

Incubating the enzyme in ^{13}CO (>99% ^{13}C, <1% ^{18}O) gives rise to the infrared spectrum shown in Figure 4B. Shown for comparison is the infrared spectrum for enzyme from the same preparation incubated in natural abundance CO (primarily ^{12}CO) (Figure 4A). Compared to the infrared spectra for enzyme flushed with natural abundance CO, the ^{13}CO-flushed enzyme exhibits new IR bands at 2027, 1951, 1925, and 1915 cm^{-1}. Bands detected in the IR spectra of the ^{12}CO spectra (at 2074, 1996, 1970, and 1959 cm^{-1}) are significantly smaller in the IR spectra of the ^{13}CO-flushed enzyme. We attribute the persistence of the ^{12}CO bands to the presence of residual natural abundance CO_2 in the enzyme buffer that is reduced to CO when the enzyme is flushed with ^{13}CO. The new 2027 cm^{-1} band in the spectra for the ^{13}CO-flushed enzyme decays at the same rate as the 2074 band of the ^{12}CO-flushed enzyme, while the new 1951 cm^{-1} band for the ^{13}CO-flushed enzyme has a decay rate similar to that of the 1996 cm^{-1} band from the ^{12}CO-flushed enzyme (data not shown). Comparison of the relative intensities and the decay rates of the bands of the ^{12}CO- and ^{13}CO-incubated enzyme samples leads to the assignment of the band shifts upon isotopic labeling with ^{13}CO shown in Table 1.

Treatment of CODH/ACS with ophen leads to 95% loss of ACS activity and 84% loss of the NiFeC EPR signal arising from cluster A, while CODH activity was relatively unaffected (see Materials and Methods), which is similar to results described earlier (*31*). Treating enzyme with ophen prior to the addition of CO also results in a dramatic and specific decrease in the intensity of the band at 1996 cm^{-1} (compare spectra A and B of Figure 5). All other IR bands detected in the untreated enzyme were largely unaffected by ophen treatment, while a weak band at 1986 cm^{-1}, which is detected as a shoulder near 1996 cm^{-1} in the untreated enzyme, can now clearly be observed in the ophen-treated enzyme. As in the untreated enzyme, the IR bands in the ophen-treated enzyme decay with time after the IR cell is loaded, with the 2074 and 1996 cm^{-1} bands being the first and last, respectively, to disappear (Figure 6).

Infrared Spectra in the Region above 2100 cm^{-1}. When CODH/ACS is incubated with ^{13}CO, besides the new bands in the spectral region between 2100 and 1800 cm^{-1} (above), a new band at 2278 cm^{-1} appears that is not detected in the ^{12}CO-flushed samples or in enzyme that has not been exposed to CO (Figure 7). The 2278 cm^{-1} band gains intensity with

Table 1: Comparison of Frequencies of ν(CO) in CODH/ACS Complexes of *M. thermoacetica* with ^{12}CO and ^{13}CO[a]

^{12}CO (cm^{-1})	^{13}CO (cm^{-1})	calcd (cm^{-1})[b]
2074	2027	2028
2044[c]	under 1996?	1999
1996	1951	1952
1970	1925	1926
1959	1915	1915
1901[c]		1859

[a] Calculated frequencies are based on a simple diatomic approximation that assumes no vibrational coupling between ν(CO) and other modes of the complex. [b] The calculated frequency is based on the equation $\nu_{13} = \nu_{12}(\mu_{12}/\mu_{13})^{1/2}$, where ν_{13} is the expected frequency of CO stretch in the ^{13}CO-flushed enzyme, ν_{12} is the observed frequency of the CO stretch in the ^{12}CO-flushed enzyme, μ_{13} is the reduced mass of the ^{13}CO molecule, and μ_{12} is the reduced mass of the ^{12}CO molecule. [c] The 1901 and 2044 cm^{-1} bands are tentatively attributed to ν(CO) modes on the basis of their detection only after the enzyme has been flushed with CO. They would be expected to shift in ^{13}CO-flushed enzyme to ca. 1999 and 1859 cm^{-1}. In neither case can a clear assignment of the ^{13}CO-shifted band be made. In the case of the 2044 cm^{-1} band, the ^{13}CO-shifted band may be obscured by the residual 1996 cm^{-1} band arising from ^{12}CO at this frequency. In the case of the 1901 cm^{-1} band, the low signal-to-noise ratio near 1859 cm^{-1} makes the detection of a band at this frequency difficult.

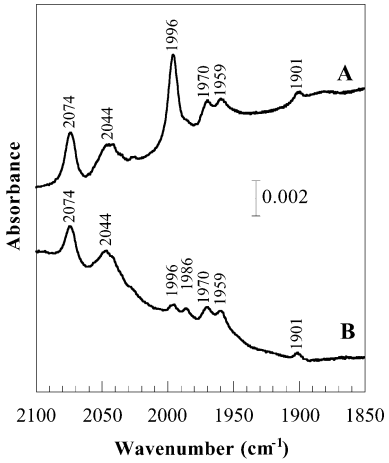

FIGURE 5: Infrared spectra of CODH/ACS from *M. thermoacetica* after addition of natural abundance CO at room temperature (A) without treatment and (B) with ophen treatment. The baselines were not corrected, nor were the spectra smoothed. However, IR bands arising from the vibration−rotation of water vapor were subtracted from the spectra. Spectra were taken 10 min after being loaded in the IR cell. The enzyme concentration was ~0.6 mM. ophen was titrated into the sample so as to reduce the NiFeC signal to 16% of the untreated sample. The specific activity for ACS activity (as measured by ^{13}CO exchange into acetyl-CoA) was reduced to 5% of the original.

incubation time after the cell is loaded and eventually levels out (Figure 7, insert).

Infrared Spectra for the 1800−1700 cm^{-1} Spectral Region. The experiments described above were performed in water-based buffers (100 mM Tris-HCl, pH 7.6, and 100 mM MES, pH 6.0). For the 50 μm path length cell used in these studies, water absorbance completely cuts off IR light below 1800 cm^{-1}. To examine the IR spectra at lower frequencies, CODH/ACS was exchanged into deuterium oxide-based buffer (100 mM MES in D_2O, pD 6.5), which allows IR data with reasonable signal-to-noise ratios to be collected in the frequency region between 1800 and 1600 cm^{-1}. While the IR spectrum in the 2100−1900 cm^{-1} region is not

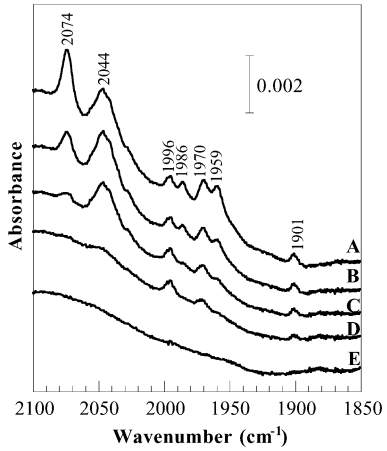

FIGURE 6: IR spectra of CO-flushed CODH/ACS that had been incubated in ophen, taken (A) 5 min, (B) 1 h, (C) 2 h, (D) 3 h, and (E) 7 h after the IR cell was filled. Spectra were taken at room temperature (512 scans, 1 cm^{-1} resolution). The baselines were not corrected, nor were the spectra smoothed. However, IR bands arising from the vibration−rotation of water vapor were subtracted from spectra taken at early times (<2 h). The enzyme concentration was 0.65 mM, and the NiFeC signal was 16% of the untreated enzyme while the specific activity for CO exchange in acetyl-CoA was reduced to 5% of the original specific activity.

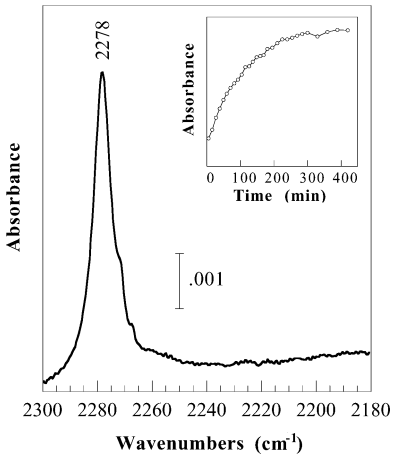

FIGURE 7: Infrared spectrum in the 2300−2180 cm^{-1} spectral region for CODH/ACS flushed with ^{13}CO. The spectrum shown was taken at room temperature 300 min after the sample was loaded into the IR cell. The enzyme concentration was 0.612 mM in 100 mM Tris-HCl buffer, pH = 7.6, with 2 mM DTT. The spectrum represents 512 scans at 1 cm^{-1} resolution. Insert: Intensity of the 2278 cm^{-1} band as a function of time after CODH/ACS was flushed with ^{13}CO.

significantly affected, two weak bands at 1727 and 1741 cm^{-1} appear when the enzyme is exchanged into this D_2O-based buffer before being treated with CO (Figure 8). These bands are not detected in enzyme samples that have not been flushed with CO. Preliminary measurements suggest that, after the IR cell is loaded, the bands at 1727 and 1741 cm^{-1} also decay, but at a slower rate than the bands in the 2100−1800 cm^{-1} spectral region (Figure 8, insert), and are still detectable after the 1996 cm^{-1} band has completely disappeared.

DISCUSSION

Exposure of CODH/ACS from *M. thermoacetica* to CO gives rise to six infrared bands at 2074, 2044, 1996, 1970, 1959, and 1901 cm^{-1} (Figure 1). A band at 1986 cm^{-1} is

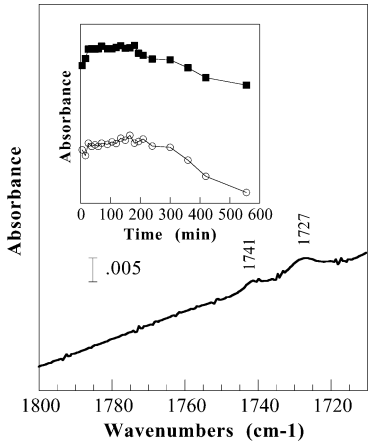

FIGURE 8: Infrared spectrum taken in the spectral region between 1710 and 1800 cm^{-1} for CODH/ACS *M. thermoacetica* after being flushed with CO. The spectrum shown was taken at room temperature 3 h after the IR cell was loaded. The enzyme concentration was 0.76 mM CODH/ACS in 100 mM MES (in D_2O), pD = 6.5. Spectra represent an average of 512 scans at 1 cm^{-1} resolution. The baselines were not corrected, nor were the spectra smoothed. Insert: Behavior of the 1741 (■) and 1727 (○) cm^{-1} bands as a function of time after being flushed with CODH/ACS with CO.

also observed when the 1996 cm^{-1} band is depleted by ophen treatment. These bands are not affected by treatment of the enzyme with EDTA, which would be expected to chelate any trace metal in the preparations that could potentially bind CO. This suggests that all the bands described above arise from CO binding to the enzyme. Both the intensities and the frequencies of these bands are consistent with their assignment to terminally bound (i.e., M−CO) metal-coordinated carbonyls, which display strong to medium intensity IR bands arising from the ν(CO) mode between 2100 and 1900 cm^{-1}. In contrast, carbonyls that bridge two metal ions exhibit IR bands significantly lower in frequency (1800−1900 cm^{-1}) (*32*). Incubation of the enzyme with ^{13}CO also supports this conclusion (Figure 4). With the possible exception of the low-intensity 1901 cm^{-1} band, all of the infrared bands detected in the ^{12}CO-flushed enzyme shift to lower frequency when the enzyme is exposed to ^{13}CO, as would be expected for a metal-bound carbonyl. The magnitude of the isotope shift agrees well with the expected shift for a vibrationally isolated ν(CO) arising from a terminally coordinated metal carbonyl (see Table 1). We therefore conclude that the six infrared bands detected upon exposing *M. thermoacetica* CODH/ACS to CO arise from the development of terminally coordinated metal carbonyls upon exposure of the enzyme to CO. The results also suggest that the CODH/ACS from *M. thermoacetica* does not contain a stable metal-coordinated carbonyl, in contrast to the proposal for an intrinsic bound CO in the *Rhodospirillum rubrum* CODH (*33*). It is somewhat surprising that, when the enzyme is exposed to 99% ^{13}CO, the IR bands arising from ^{12}CO treatment are still observed, albeit at reduced intensity. It is likely that these bands arise from natural abundance CO_2 and bicarbonate ("CO_2") that are dissolved in the enzyme solution and are reduced to ^{12}CO when the enzyme is exposed to ^{13}CO.

Since cluster C on CODH and cluster A on ACS are both involved in CO metabolism, IR bands would be expected at both of these sites. Earlier, a band at 1995 cm^{-1} (1951 cm^{-1} in ^{13}CO) was observed in CO-incubated enzyme and was assigned as a terminal CO bound to a metal center in cluster A of ACS because the 1951 cm^{-1} band was replaced with the 1995 cm^{-1} band when $CH_3{}^{12}CO$-CoA was incubated with the ^{13}CO-treated enzyme (*12*). To further study CO binding to clusters A and C and to discriminate between CO binding to cluster C versus CO binding to cluster A, we have examined the pattern of IR bands detected in enzyme treated with ophen under conditions where the ACS activity (as measured by the CO/acetyl-CoA exchange reaction) and the "NiFeC" EPR signal arising from cluster A are both significantly reduced, while the CODH activity and EPR signals arising from cluster C are largely unaffected. Under these conditions, the 1996 cm^{-1} band decreases significantly in intensity, while the bands at 2074, 2044, 1970, 1959, and 1901 cm^{-1} remain (Figure 5),[2] indicating that the 1996 cm^{-1} band arises from CO binding to a metal ion in cluster A that is removed or significantly altered by ophen treatment. Coincidence of the rates of decay of the NiFeC EPR signal and the 1996 cm^{-1} IR band provides further evidence that this band arises from a M−CO complex at cluster A, as suggested earlier (*12*). Loss of the CO/acetyl-CoA exchange activity concomitant with loss of the 1996 cm^{-1} band further suggests that this terminally coordinated metal−CO species is catalytically relevant to acetyl-CoA synthase activity. The remaining CO bands (i.e., 2074, 2044, 1970, 1959, and 1901 cm^{-1}) are tentatively assigned as arising from carbonyls bound to cluster C, although given the multiple metal ions now known to occupy the proximal metal site in cluster A (Cu, Ni, and Fe), the possibility that at least one of these bands might arise from CO binding to other metal ions at cluster A cannot be excluded. Another possibility is that at least one of those bands (most likely the 2044 cm^{-1} band due to the lag in its decay) could arise from an EPR-silent complex of the A cluster with CO. IR studies with the monofunctional CODH would help to resolve this issue.

Conversion of CO to CO_2 in the IR Cell. All IR bands arising from metal carbonyls observed in these studies decay with time (Figures 2, 3, and 6). In all samples studied, the 2074 cm^{-1} band, which is attributable to a metal−carbonyl bound to cluster C, first loses intensity. The IR bands at 2044, 1970, and 1959 cm^{-1}, which are also tentatively attributed to metal carbonyls at cluster C, also decay rapidly as the time after loading the IR cell elapses. Interestingly, the bands at 2074, 1970, 1959, and 1901 cm^{-1} exhibit decays that are linear in time, indicating zero-order kinetics. In contrast, the intensity of the 1996 cm^{-1} band, which is attributed to a metal carbonyl at cluster A (above), remains stable until all of the other IR bands in the IR spectra disappear. Furthermore, while significant decay of the M−CO bands occurs in the IR cell during the first 1−2 h after the enzyme is incubated with CO, when the enzyme is incubated in an anaerobic vial with a large CO headspace (>100 times the sample volume) for 1−2 h prior to the IR cell being loaded, the rate at which the IR bands disappear is the same as when the enzyme is flushed with CO and immediately loaded into the IR cell. The difference is that enzyme in the anaerobic vial has significantly more available CO due to the large

[2] The small residual 1996 cm^{-1} band remaining after ophen treatment is consistent with a small amount of ACS activity remaining in these samples following the addition of ophen.

headspace of CO gas compared to the enzyme in the IR cell, which lacks a CO headspace. These combined results strongly indicate that the time-dependent decay of these IR bands arises from in situ conversion of CO into CO_2 and H_2 by CODH (eq 4).

$$CO + H_2O \rightarrow CO_2 + H_2 \quad (4)$$

The hypothesis that the M−CO bands decay due to CO oxidation is consistent with the observation that highly purified CODH/ACS from *M. thermoacetica* exhibits an appreciable CO-dependent hydrogen evolution activity in the absence of electron acceptors with a rate constant of 90 min^{-1} at 25 °C and pH = 6.0 (590 $nmol^{-1}$ min^{-1} mg^{-1}) (*34*). Accordingly, in our simulations of the EPR signal and the 1996 cm^{-1} band, CO_2 formation occurs at a rate of ∼30 min^{-1} at room temperature and pH = 7.6. Since the IR transmission cell has no headspace for CO gas, the amount of CO present in the cell is limited to the CO in solution at the time the IR cell is loaded (∼1 mM), which would be rapidly depleted and eventually lead to the loss of all metal carbonyls in CODH/ACS and all the CO in solution.

The proposal that depletion of the IR bands results from conversion of CO to CO_2 and H_2 is supported by the observation that enzyme that has been incubated with ^{13}CO elicits a new IR band at 2278 cm^{-1}, which gradually gains intensity over the course of the experiment. Dissolved $^{13}CO_2$ is expected to elicit an IR band near 2278 cm^{-1} (*35*), while dissolved $^{12}CO_2$ would be expected to give rise to IR frequencies near 2349 cm^{-1} (*36*). Unfortunately, dissolved $^{12}CO_2$ cannot be reliably confirmed since the spectrometer itself has significant residual natural abundance CO_2, which would be expected to obscure any bands arising from the formation of dissolved $^{12}CO_2$. The enzyme solution also probably contains some dissolved "$^{12}CO_2$", since the atmospheric CO_2 concentration is ∼0.03%. We suggest that the bands at 1724 and 1741 cm^{-1} (Figure 8) might also arise from the in situ conversion of CO into CO_2. Metal-bound carboxylates (M−CO_2) are known. Of particular interest are the known Ni−CO_2 species, where the CO_2 molecule is bent and is coordinated to the metal in a side-on fashion through both the carbon and the oxygen. These complexes display two IR-active modes arising from the C−O stretch, an asymmetric mode with frequencies between 1760 and 1660 cm^{-1} and a symmetric mode with frequencies between 1210 and 1150 cm^{-1} (*32*, *37*). As far as we know, the IR spectra of metal-coordinated carboxylic acids (M−COOH), which might be formed in the enzyme-catalyzed conversion of CO into CO_2, have not been reported; thus, the ν(CO) frequency of such a complex is unknown. Organic carboxylic acids (RCOOH) also have ν(CO) bands between 1760 and 1700 cm^{-1}(*38*), which raises the possibility that one of these bands might arise from a metal-coordinated carboxylic acid. Further experiments are currently underway to determine the nature of the species producing these bands.

The lag phase and time-dependent loss of the 1996 cm^{-1} band, which has been attributed to a metal carbonyl at cluster A, are also consistent with the depletion of CO from the enzyme solution and IR cell as cluster C converts CO into CO_2. In this case, as the CO is depleted from solution, the equilibrium between the CO bound (M−CO) and unbound forms (M + CO) of cluster A is shifted more and more toward the unbound form, so that eventually all of the CO would be released from cluster A and subsequently converted into CO_2 at cluster C. Similar lag phases and decay curves are observed for the 1996 cm^{-1} IR band and for the NiFeC signal associated with CO binding to cluster A. When the amount of CO available to the enzyme is limited to what is available in solution (conditions comparable to those of the IR experiments), the intensity of the NiFeC signal is at first stable but then decays with a half-life of approximately 55 min (Figure 3).

The Nature of CO Binding at Cluster A. As discussed above, the IR band detected at 1996 cm^{-1} upon incubating CODH/AC with CO is attributable to the formation of a metal carbonyl at cluster A. Examination of the X-ray crystallographic structure of the CODH/ACS from *M. thermoacetica* suggests that the CO binds to either the square-planar distal Ni ion that is coordinated to two backbone N's and two cysteine thiolates to the tetrahedrally coordinated Cu ion (the proximal metal) that is coordinated to three cysteine thiolates and an unidentified nonprotein ligand (*4*) or to a Ni ion that can occupy the Cu site (*3*). The Fe ions of cluster A are coordinatively saturated, forming a classical cubane, and are less likely candidates to bind CO. We summarize here what is known about the infrared stretching frequency, ν(CO), for Ni(I)−CO and Cu(I)−CO complexes. Terminally coordinated carbonyl complexes of Cu(I) containing sulfur and/or nitrogen ligation display ν(CO) values between 2180 and 2055 cm^{-1} (*39*). The Cu(I) carbonyl in [Cu([9]aneS_3)CO][PF_6] (containing three thioether ligands) displays a ν(CO) of 2081 cm^{-1}, while the [LCu(CO)][PF6] complex [L = *N*-[2-(1-naphthyl)ethyl]-1-aza-4,8-dithiacyclodecane] in which Cu is coordinated to two thioethers and a nitrogen displays a ν(CO) of 2101 cm^{-1} (*40*, *41*). Additionally, the CO-bound form of Cu_B(I) in cytochrome *c* oxidase (in which the Cu ion is ligated to the enzyme via three histidines) displays a ν(CO) of 2061 cm^{-1} (*42*, *43*). Hence, the ν(CO) for known Cu(I)−CO complexes are significantly higher than the 1996 cm^{-1} band detected for CO binding at cluster A. In contrast, Ni(I) carbonyls have, in general, somewhat lower frequencies; for instance, [PhTt^{tBu}]−Ni^{I}−CO (in which the Ni is coordinated to three thioethers) has a ν(CO) of 1999 cm^{-1} while the [Ni^{I}(DAPA)-(SPh_2)$_2$(CO)]$^-$ (containing two thiolate and two nitrogen ligands) has a ν(CO) of 2040 cm^{-1} (*41*, *44*). For comparison, the stable, CO-inhibited, EPR-silent form of the [NiFe] hydrogenase isolated from *Allochromatium vinosum* (Ni−S−CO), generally believed to be a Ni(II)−CO species (coordinated to four cysteine thiolates), displays a ν(CO) of 2060 cm^{-1} (*45*). Hence, the 1996 cm^{-1} band attributable to CO binding at cluster A is somewhat more similar to known Ni(I)−CO models. CO binding to Ni(I) is also supported by the ophen experiments since removal of Ni causes loss of ACS activity and NiFeC signal intensity, which are restored upon reconstitution with Ni (here and ref *31*). ophen does not remove Cu from the A cluster, which strongly suggests that the 1996 cm^{-1} band does not derive from a Cu(I)−CO (unpublished results). These results indicate that the Ni−Ni form of ACS, with Ni at both the "Cu site" and the carboxamide (N_2S_2) sites, is the state that binds CO and tentatively support the conclusion (*3*) that the Ni−Ni form is the active state of ACS.

The Nature of CO Binding at Cluster C. No IR bands are observed in the 2100−1900 cm^{-1} spectral region for the as-isolated CODH/ACS from *M. thermoacetica*, and all of the IR bands attributable to metal carbonyls on cluster C decay fairly rapidly. Thus, the CODH from *M. thermoacetica* does not contain stable intrinsic CO ligands at cluster C, which challenges the proposal that two CO are bound to the CODH site of *R. rubrum* before CO is added (*33*). However, at least four different IR bands (2074, 2044, 1970, and 1959 cm^{-1} and, potentially, a fifth at 1901 cm^{-1}), which are attributable to metal carbonyls in cluster C, develop upon incubation of CODH/ACS with CO. The large number of bands detected upon flushing the enzyme with CO is difficult to understand in terms of the currently proposed models for CO binding and turnover. Heterogeneity in the sample arising from a variation in redox states for the CO binding site at cluster C might conceivably account for some of these IR bands. For example, EPR spectra of CODH reveal that only ∼30% of the enzyme is in the so-called Cred2 state, indicating that both diamagnetic and paramagnetic states of the C cluster are present. Sample-to-sample heterogeneity is consistent with the observation that the 1901 and 2044 cm^{-1} band intensities are somewhat preparation dependent. It may also account for the vast difference in the frequencies between some of the bands detected at cluster C, since a difference in oxidation state would be expected to alter ν(CO) dramatically (approximately 80−100 cm^{-1} for a 1 unit change in oxidation state). However, it is difficult to imagine that all of the IR bands detected in these studies arise from heterogeneity in a single CO binding site at cluster C, with a relatively small number of physiologically relevant redox states available to it. This leaves open the interesting possibility that there is more than one CO binding site in cluster C. Such a scenario is consistent with kinetic experiments indicating that 2 mol of CO react during a single catalytic cycle of CO oxidation (*46*). The binding of one or more CO at cluster C may also be required to poise the active site in the correct redox state for the eventual binding and turnover of CO. Furthermore, potential open coordination sites are present at both the Ni center and the extrinsic Fe atom [called ferrous component II (*9*)].

CONCLUSIONS

Infrared studies on the ^{12}CO- and ^{13}CO-incubated bifunctional CODH/ACS from *M. thermoacetica* provide direct evidence that CO binds to metal ions in both clusters A and C. An IR band at 1996 cm^{-1} is attributed to formation of a metal carbonyl at cluster A. The assignment of the 1996 cm^{-1} band as arising from CO binding at cluster A is based on the disappearance of this band when the enzyme is treated with ophen and the disappearance of this band at the same rate as loss of the NiFeC EPR signal. The frequency of this band is most similar to ν(CO) for known Ni(I) carbonyls.

No IR bands are detected in the 2100−1900 cm^{-1} spectral region for as-isolated CODH/ACS, while incubating the enzyme with CO elicits as many as five different IR bands in this region, which are attributable to the formation of metal carbonyls at cluster C. These results strongly suggest that the bifunctional enzyme from *M. thermoacetica* does not contain intrinsic carbonyl ligands in cluster C, as has been proposed in the monofunctional CODH from *R. rubrum*. All of the IR bands associated with CO binding to cluster C (as well as the 1996 cm^{-1} band assigned to cluster A) decay over time. Correspondingly, the IR bands disappear when CODH/ACS is preincubated with CO and then allowed to rest. The decay curves were fit to a model including the in situ conversion of CO to CO_2 (with the concomitant formation of hydrogen). Formation of CO_2 in the IR cell despite the absence of an added external electron acceptor is supported by the detection of a band attributable to dissolved $^{13}CO_2$ when the enzyme is flushed with ^{13}CO. IR bands that are potentially attributable to metal carboxyls or metal carboxylates are also detected.

Finally, the finding that multiple IR bands attributable to metal carbonyls on cluster C are detected upon exposure of the enzyme to CO leaves open the possibility that more than one CO binding site may be present at cluster C. Examination of the crystal structure of the C cluster active site for the monofunctional CODH's from *R. rubrum* and *Clostridium hydrogenoformans* suggests that open ligation sites may exist on both the Ni and Fe ions of this unusual NiFeS cluster. Further studies are currently underway to test this possibility.

REFERENCES

1. Ragsdale, S. W. (2003) in *Encyclopedia of Catalysis* (Horvath, I. T., Iglesia, E., Klein, M. T., Lercher, J. A., Russell, A. J., and Stiefel, E. I., Eds.) pp 665−695, John Wiley and Sons, New York.
2. Lindahl, P. A. (2002) *Biochemistry 41*, 2097−2105.
3. Darnault, C., Volbeda, A., Kim, E. J., Legrand, P., Vernade, X., Lindahl, P. A., and Camps, J. C. F. (2003) *Nat. Struct. Biol. 10*, 271−279.
4. Doukov, T. I., Iverson, T., Seravalli, J., Ragsdale, S. W., and Drennan, C. L. (2002) *Science 298*, 567−572.
5. Bott, M., Eikmanns, B., and Thauer, R. K. (1986) *Eur. J. Biochem. 159*, 393−398.
6. Khahlil, M. A. K., Pinto, J. P., and Shearer, M. J. (1999) *Chemosphere: Global Change Sci. 1*, ix−xi.
7. King, G. M., and Hungria, M. (2002) *Appl. Environ. Microbiol. 68*, 4480−4485.
8. Meyer, O. (1985) in *Microbial Gas Metabolism, Mechanistic, Metabolic, and Biotechological Aspects* (D., R. K. P., and C. S., Eds.) pp 131−151, Academic Press, London.
9. Meyer, O., Frunzke, K., and Morsdorf, G. (1993) in *Microbial Growth on C, compounds* (Murell, J. C., and Kelly, D. P., Eds.), Intercept Ltd., Andover, U.K.
10. Menon, S., and Ragsdale, S. W. (1996) *Biochemistry 35*, 12119−12125.
11. Ragsdale, S. W., Kumar, M., Zhao, S., Menon, S., Seravalli, J., and Doukov, T. (1998) in *Vitamin B12 and B12 Proteins* (Krautler, B., Ed.) pp 167−177, Wiley-VCH, Weinham, Germany.
12. Kumar, M., and Ragsdale, S. W. (1992) *J. Am. Chem. Soc. 114*, 8713−8715.
13. Bagley, K. A., Duin, E. C., Roseboom, W., Albracht, S. P. J., and Woodruff, W. H. (1995) *Biochemistry 34*, 5527−5535.
14. Volbeda, A., Garcin, E., Piras, C., deLacey, A. L., Fernandez, V., Hatchikian, V. M., Frey, M., and Fontecilla-Camps, J. C. (1996) *J. Am. Chem. Soc. 118*, 12989−12996.
15. Happe, R. P., Roseboom, W., Pierik, A. J., Albracht, S. P. J., and Bagley, K. A. (1997) *Nature 385*, 126.
16. Van Der Spek, T. M., Bagley, K. A., Arendsen, A. F., Happe, R. P., Yun, S., Bagley, K. A., Stufkens, D. J., Hagen, W. R., and Albracht, S. P. J. (1996) *Eur. J. Biochem. 237*, 629−634.
17. De Lacey, A. L., Stadler, C., Cavazza, C., Hatchikian, E. C., and Fernandez, V. M. (2000) *J. Am. Chem. Soc. 122*, 11232−11233.
18. Chen, Z., Lemon, B. J., Huang, S., Swartz, D. J., Peters, J. W., and Bagley, K. A. (2002) *Biochemistry 41*, 2036−2043.
19. Caughey, W. S., Shimada, H., Choc, M. G., and Tucker, M. P. (1981) *Proc. Natl. Acad. Sci. U.S.A. 78*, 2903−2907.
20. Johnson, J. B., Lamb, D. C., Frauenfelder, H., Muller, J. D., McMahon, B., Nienhaus, G. U., and Young, R. D. (1996) *Biophys. J. 71*, 1563−1573.
21. Muller, J. D., McMahon, B. H., Chien, E. Y., Sligar, S. G., and Nienhaus, G. U. (1996) *Biophys. J. 71*, 1563−1573.
22. Franzen, S. (2002) *J. Am. Chem. Soc. 124*, 13271−13281.

23. Bailey, J. A., Tomson, F. L., Mecklenburg, S. L., MacDonald, G. M., Katsonouri, A., Puustinen, A., Gennis, R. B., Woodruff, W. H., and Dyer, R. B. (2002) *Biochemistry 41*, 2675−2683.
24. Andreesen, J. R., Schaupp, A., Neurater, C., Brown, A., and Ljungdahl, L. G. (1973) *J. Bacteriol. 114*, 743−751.
25. Ragsdale, S. W., Clark, J. E., Ljungdahl, L. G., Lundie, L. L., and Drake, H. L. (1983) *J. Biol. Chem. 258*, 2364−2369.
26. Russell, W. K., Stalhandske, C. M. V., Xia, J. Q., Scott, R. A., and Lindahl, P. A. (1998) *J. Am. Chem. Soc. 120*, 7502−7510.
27. Shin, W., and Lindahl, P. A. (1992) *Biochemistry 31*, 12870−12875.
28. Ragsdale, S. W., and Wood, H. G. (1985) *J. Biol. Chem. 260*, 3970−3977.
29. Barshop, B. A., Wrenn, R. F., and Frieden, C. (1983) *Anal. Biochem. 133*, 134−145.
30. Ragsdale, S. W., Wood, H. G., and Antholine, W. E. (1985) *Proc. Natl. Acad. Sci. U.S.A. 82*, 6811−6814.
31. Shin, W., Anderson, M. E., and Lindahl, P. A. (1993) *J. Am. Chem. Soc. 115*, 5522−5526.
32. Nakamoto, K. (1997) *Infrared and Raman Spectra of Inorganic and Coordination Compunds, Part B: Applications in Coordination, Organometallic, and Bioinorganic Chemistry*, 5th ed., John Wiley and Sons, New York.
33. Heo, J., Staples, C. R., Halbieb, C. M., and Ludden, P. W. (2000) *Biochemistry 39*, 7956−7963.
34. Menon, S., and Ragsdale, S. W. (1996) *Biochemistry 35*, 15814−15821.
35. Nielson, A. H., and Lagermann, R. J. (1954) *J. Chem. Phys. 22*, 36−39.
36. Taylor, J. H., Benedict, W. S., and Strong, J. (1952) *J. Chem. Phys. 20*, 1884−1898.
37. Busca, G., and Lorenzelli, V. (1982) *Mater. Chem. 7*, 89−126.
38. Nakanishi, K., and Solomon, P. H. (1977) *Infrared Absorption Spectroscopy*, Holden-Day, Oakland, CA.
39. Hathaway, B. J. (1987) in *Comprehensive Coordination Chemistry: The Synthesis, Reactions, Properties, and Applications of Coordination Compounds* (Wilkinson, G., Gillard, R. D., and McCleverty, J. A., Eds.) pp 533−774, Pergamon Press, New York.
40. Conry, R. R., Striejewske, and Tipton, A. A. (1999) *Inorg. Chem. 38*, 2833−2843.
41. Hirsch, J., DeBeer, G. S., Solomon, E. I., Hedman, B., Hodgson, K. O., and Burstyn, J. N. (2001) *Inorg. Chem. 40*, 2439−2441.
42. Alben, J. O., Moh, P. P., Fiamingo, F. G., and Altschuld, R. A. (1981) *Proc. Natl. Acad. Sci. U.S.A. 78*, 234−237.
43. Dyer, B. R., Einarsdotir, O., Killough, P. M., Lopez-Garriga, J. J., and Woodruff, W. H. (1989) *J. Am. Chem. Soc. 111*, 7657−7659.
44. Schebler, P. J., Mandimutsira, B. S., Riordan, C. G., Liable-Sands, L. M., Incarvito, C. D., and Rheingold, A. (2001) *J. Am. Chem. Soc. 123*, 331−332.
45. Bagley, K. A., Van Garderen, C. J., Chen, M., Duin, E. C., Albracht, S. P. J., and Woodruff, W. H. (1994) *Biochemistry 33*, 9929−9236.
46. Seravalli, J., Kumar, M., Lu, W.-P., and Ragsdale, S. W. (1997) *Biochemistry 36*, 11241−11251.

BI0349470